JOURNAL OF GEOPHYSICAL RESEARCH, VOL. 114, B03301, doi:10.1029/2008JB005975, 2009

Modeling 3-D wave propagation and finite slip for the 1998 Balleny Islands earthquake

Vala Hjörleifsdóttir,[1,2] Hiroo Kanamori,[1] and Jeroen Tromp[1,3]

Received 31 July 2008; revised 22 November 2008; accepted 11 December 2008; published 4 March 2009.

[1] We simulate surface waves in a 3-D Earth model using a spectral element method for existing kinematic source models of the M_W 8.1, 25 March 1998 Balleny Islands earthquake. The 3-D model incorporates lateral variations in the crust and mantle on the basis of models Crust2.0 and S20RTS. Our objective is to investigate the fit of the observed and simulated long-period surface waves in the hope of improving on the existing source models. We modify a body wave model determined by Henry et al. (2000) to improve the fit of long-period surface waveforms. We demonstrate that adding a smooth component of slip extending over a fault that connects the two subevents determined by Henry et al. (2000), without invoking slip on multiple fault planes or on unconnected fault patches, provides reasonable fits to long-period surface waves as well as body waves.

Citation: Hjörleifsdóttir, V., H. Kanamori, and J. Tromp (2009), Modeling 3-D wave propagation and finite slip for the 1998 Balleny Islands earthquake, *J. Geophys. Res.*, *114*, B03301, doi:10.1029/2008JB005975.

1. Introduction

[2] The last decades have seen significant advances in finite source earthquake modeling. Early models based on long-period surface waves described the rupture process in terms of the source dimensions, duration, uniform slip, and a constant rupture speed [*Ben-Menahem*, 1961]. By considering the details of high-frequency body waveforms, *Kikuchi and Kanamori* [1991] characterized rupture in terms of individual subevents, each with their own location, timing, mechanism, and duration. However, band-limited body wave recordings are not sensitive to long-period slip, and the scalar moment is often underestimated. In contrast, surface waves are not as sensitive to details of the slip history, but for moderate-sized events they are sensitive to the scalar moment. To match surface and body waveforms simultaneously, subevent models have been augmented by a component of slip over the whole fault plane [*Kikuchi and Fukao*, 1987]. *Ekström* [1989] combined long- and short-period data to invert for a propagating unilateral rupture. With the advent of broadband data, there has been an explosion in the use of body waveforms to generate maps of slip on fault planes [see, e.g., *Hartzell and Heaton*, 1983]. Similar maps may be generated using long-period surface waves, but they are typically much less detailed, because only very long period seismograms that are less sensitive to 3-D structure can be reliably utilized. Improved, more detailed slip models will enable seismologists to answer questions about the continuity and complexity of rupture, gradients in slip, and interaction between separate slip patches on the same fault plane.

[3] Despite the high quality of modern broadband records of ground motion, it still holds true that body waves are inherently insensitive to long-period aspects of rupture, and thus any complete modeling of an earthquake should include measurements that are more sensitive to long-period characteristics of the source process. Because surface waves are sensitive to shallow 3-D heterogeneity in the crust and upper mantle, care has to be taken when using them to constrain kinematic rupture models. To accurately account for such lateral heterogeneity is computationally expensive, and therefore it is difficult to include surface waves directly in kinematic source inversions. With currently available open-source tools to accurately compute complete synthetic seismograms in 3-D Earth models [*Komatitsch and Tromp*, 2002a, 2002b], it is becoming viable to assess the surface wave fit of kinematic source models determined from broadband body wave data. In this paper we describe how using an a priori body wave model and only a handful of 3-D simulations, one may obtain a finite source model that simultaneously matches body and surface wave seismograms, thus providing a self-consistent description of the source.

[4] We illustrate the method for the M_W 8.1, 25 March 1998 earthquake in the Antarctic plate. This event is far from labeled geographical locations, but is often named after the Balleny Islands, which are over 700 km to the southeast. The earthquake has been studied extensively by many authors because it exhibits a number of peculiarities. The tectonic forces responsible for this earthquake are not immediately obvious. The event occurred on a fault about 300 km from the nearest plate boundary (Figure 1), and most models indicate slip on a fault plane perpendicular to the fracture zones in this region. Because of sparse instru-

[1] Seismological Laboratory, Division of Geological and Planetary Sciences, California Institute of Technology, Pasadena, California, USA.
[2] Now at Lamont-Doherty Earth Observatory, Palisades, New York, USA.
[3] Now at Department of Geosciences, Princeton University, Princeton, New Jersey, USA.

0148-0227/09/2008JB005975$09.00

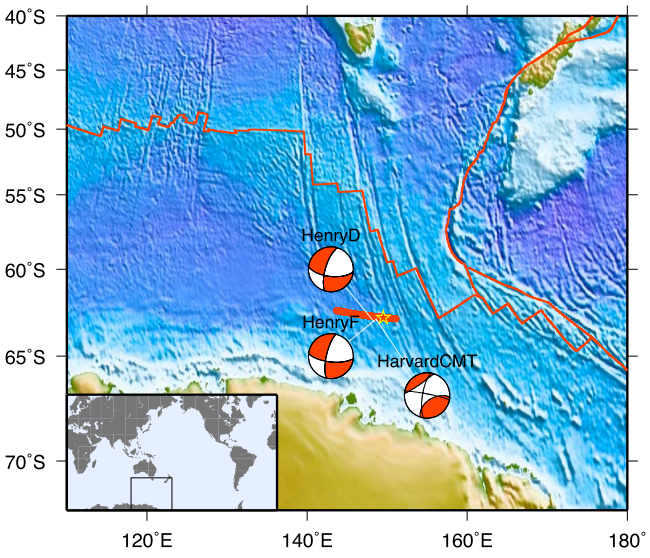

Figure 1. The Balleny Islands earthquake occurred relatively far from plate boundaries (thin red lines), and most researchers agree that the fault plane is close to perpendicular to the plate fabric. We use source models determined by *Henry et al.* [2000] (HenryD and HenryF) and the Harvard CMT to calculate 3-D synthetic seismograms.

mentation in the southern hemisphere, kinematic source inversions are challenging; still, many slip models have been determined from body waveforms [*Kuge et al.*, 1999; *Nettles et al.*, 1999; *Antolik et al.*, 2000; *Henry et al.*, 2000; *Tsuboi et al.*, 2000]. The Harvard Centroid Moment Tensor (CMT) solution has a large non-double-couple component (see Figure 1) that *Kuge et al.* [1999] explain in terms of slow slip on a normal fault and *Antolik et al.* [2000] interpret as a compound rupture of a normal fault and a strike slip fault. One of the more detailed body wave source models [*Henry et al.*, 2000] has a 100 km stretch of no slip between two distinct fault patches (Figure 4), and therefore it is difficult to explain the mechanics of fault rupture with the standard mechanism in which rupture propagation is driven by stress concentration at a crack tip. Here we compute 3-D synthetic seismograms at Global Seismographic Network (GSN) stations, for various source models of the Balleny Islands earthquake, and quantify and interpret the misfits between synthetic and observed surface waves. In particular, we simulate surface waves for the body wave finite source model presented by *Henry et al.* [2000] to investigate whether this model, without a non-double-couple component, can explain the observations.

2. Data Retrieval and Processing

[5] We retrieved seismograms from most permanent global stations recording one-sample-per-second broadband data, which are archived at the IRIS Data Management Center www.iris.edu). We remove the instrument response from the records using deconvolution to obtain ground displacement. For each model we calculate synthetic waveforms using a spectral element method (SEM) [*Komatitsch and Tromp*, 2002a, 2002b]. We use a 3-D Earth model that combines mantle model S20RTS [*Ritsema et al.*, 1999] and crustal model Crust2.0 [*Bassin et al.*, 2000]. The 3-D SEM synthetics incorporate the effects of gravity, rotation, topography and bathymetry, the oceans, and attenuation.

[6] We limit our attention to the period range between 40 s and 500 s. The upper bound is determined by the signal-to-noise ratio at long periods and the lower bound reflects the shortest period where the 3-D synthetics can accurately reproduce the observed records.

3. Quantifying the Quality of a Source Model

[7] We compare different earthquake source models and wish to determine which ones satisfactorily predict the observed seismograms. The quality of a prediction may be defined in terms of a measure of misfit between observed and synthetic seismograms. To understand the cause of mismatch between data and synthetics, it is helpful to quantify this misfit in terms of frequency-dependent time shifts and amplitude anomalies. In the frequency domain, we write the observed seismogram as $d(\omega)$ and the synthetic seismogram as $s(\omega)$, where ω denotes the angular frequency. We define the transfer function between the two, $T(\omega)$, such that when applied to the synthetic it minimizes the waveform misfit to the observed seismogram:

$$|d(\omega) - T(\omega)s(\omega)|^2 = \text{minimum}. \tag{1}$$

The choice of time window used for comparing data and synthetics can influence the frequency-dependent measurements due to spectral leakage, since windowing in the time domain corresponds to convolution in the frequency domain. To minimize spectral leakage, we choose a windowing function, or taper, that has compact support in the frequency domain. Unfortunately, such compactly supported tapers apply nonequal weights along the length of the window, causing a bias. To reduce this bias we use a multitaper measurement technique involving multiple orthogonal time windows [*Thomson*, 1982], each of which has a different bias, and average the results. It can be shown that the first $2k = 2LW$ prolate spheroidal eigen tapers [*Slepian*, 1978] for a time series of length L, are optimally concentrated within a window W in the frequency domain. An added benefit of using multiple tapers is that, since we get several estimates for each spectral measurement, we can compute the average and the dispersion in the estimate.

[8] Following *Laske and Masters* [1996] and *Zhou* [2004], the transfer function $T(\omega)$ may be obtained by using $2k$ prolate spheroidal eigen tapers $h_j(\omega)$, $j = 1,\ldots,2k$. We define $\mathbf{d}(\omega) = [d_1(\omega),.., d_j(\omega),.., d_{2k}(\omega)]^T$ as the $2k$-dimensional vector that contains the $2k$ spectral estimates $d_j(\omega) = d(\omega) \otimes h_j(\omega)$, where $\otimes$ denotes convolution. We similarly define $\mathbf{s}(\omega) = [s_1(\omega),.., s_j(\omega),.., s_{2k}(\omega)]^T$. In terms of the eigen tapers, the solution to (1) is given by $\mathbf{s}^T[\mathbf{d} - T\mathbf{s}] = \mathbf{0}$, i.e.,

$$T = \frac{\sum_{j=1}^{2k} d_j s_j^*}{\sum_{j=1}^{2k} s_j s_j^*}, \tag{2}$$

which is how we obtain the transfer function given the data and the synthetic. Here * denotes the complex conjugate.

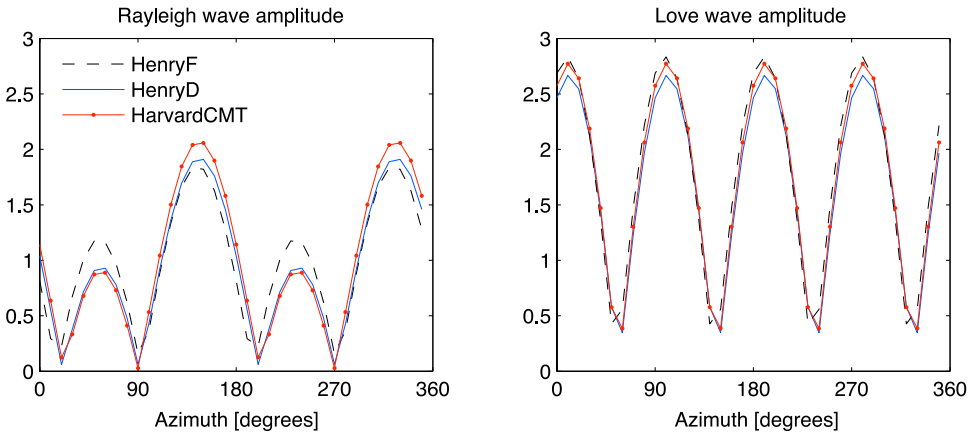

Figure 2. Radiation patterns for three different unit point sources computed at a dominant period of 256 s. Notice that the HenryD model and the Harvard CMT solution are nearly indistinguishable, whereas the model HenryF has slightly larger amplitude Rayleigh waves between 20°–90° and 200°–270°.

We may express the complex transfer function T in terms of a real, frequency-dependent time shift $\delta\tau$ and a real, frequency-dependent amplitude anomaly $\delta \ln A$ as

$$T = (1 + \delta \ln A) \exp(-i\omega\delta\tau), \tag{3}$$

where

$$\delta\tau = -\frac{1}{\omega} \tan^{-1}\left(\frac{\mathrm{Im}T}{\mathrm{Re}\,T}\right), \tag{4}$$

$$\delta \ln A = |T| - 1. \tag{5}$$

The frequency-dependent time shift (4) and amplitude anomaly (5) are the measures of misfit we will be using. To make the multitaper measurements we use an 800 s window centered on $t = \Delta/3.8$ km/s for Rayleigh waves and $t = \Delta/4.3$ km/s for Love waves, where Δ is the epicentral distance. We use the first five 2.5π prolate spheroidal tapers to estimate the transfer function. This choice leads to independent estimates of the true spectra every $2.5/L$ Hz, where L is the length of the time series; that is, every 2.5/800 s = 0.003125 Hz.

[9] The transfer function tells us how to amplify and shift each frequency component in order to best fit the data. If the data and synthetics are similar to start with, the reconstructed synthetic will be nearly identical to the data. If the traces are dissimilar, there is no way to shift and multiply the different frequency components to make the traces look like each other. We use the normalized waveform misfit defined as $||d - s||^2/||d||^2$ and the amplitude anomalies $||d||/||s|| - 1$ to quantify the differences between the original seismograms and the reconstructed synthetics, where $||d||^2 = \int_0^T d(t)^2\, \mathrm{d}t$. We only retain measurements when the normalized waveform misfit between the data and reconstructed synthetic is smaller than 0.3 and the amplitude anomalies are 0.2 or smaller.

[10] Each multitaper measurement gives us an estimate of the time shift, $\delta\tau_i(\omega)$, and the amplitude anomaly, $\delta \ln A_i(\omega)$, at station i and angular frequency ω. This provides us with a large number of measurements for each model. In order to visualize the results we can combine the measurements. We define the average over all measurements by

$$\overline{\delta\tau} = \frac{1}{N} \sum_{i=1}^{N} \frac{1}{\omega_1 - \omega_0} \int_{\omega_0}^{\omega_1} \delta\tau_i(\omega)\mathrm{d}\omega, \tag{6}$$

and we define the variations around the average over all measurements by

$$\sigma^{\tau} = \left\{ \frac{1}{N} \sum_{i=1}^{N} \frac{1}{\omega_1 - \omega_0} \int_{\omega_0}^{\omega_1} [\delta\tau_i(\omega) - \overline{\delta\tau}]^2 \mathrm{d}\omega \right\}^{\frac{1}{2}}, \tag{7}$$

where N is the total number of stations and ω_0 and ω_1 are the lowest and highest angular frequencies of interest. For the amplitudes we define $\overline{\delta \ln A}$ and $\sigma^{\ln A}$ in a similar fashion.

4. Point Source Models

[11] We compute the radiation pattern as described by *Ben-Menahem and Harkrider* [1964] and *Kanamori and Given* [1981] for three unit point sources (Figure 1): the Harvard CMT solution [*Dziewonski et al.*, 2003] and the "HenryD" and "HenryF" models of *Henry et al.* [2000, Table 1] (solutions D and F, respectively). The Harvard CMT and HenryD models were obtained from mantle waves at periods of 135 s and longer, whereas model HenryF was determined from body waves filtered between periods of 2 s and 120 s. The source parameters are summarized in Table 1. The moment tensor elements are normalized such that the full moment tensor is given by $\mathbf{M} = M_0\mathbf{m}$, where $M_0^2 = (\mathbf{M}{:}\mathbf{M})/2$ defines the scalar moment. The timing of the best fit point source, relative to the hypocentral time, is given by t_0 in Table 1. The radiation patterns are shown in Figure 2. The differences between mechanism HenryF and the other two mechanisms are small but evident for the smaller lobes of the radiation pattern, between 20°–90° and 200°–270°. The radiation pattern for the Harvard CMT solution and the HenryD model are very similar, and it would be very difficult to distinguish between them from surface wave amplitudes alone if there was noise in the data. We therefore

Table 1. Comparison of Focal Mechanisms Used to Model the Balleny Islands Earthquake

	Model		
	Harvard CMT	HenryD	HenryF
M_0 (N m)	$1.86 \cdot 10^{21}$	$1.30 \cdot 10^{21}$	$1.40 \cdot 10^{21}$
m_{rr}	−0.3557	−0.3079	−0.2068
$m_{\theta\theta}$	0.4959	0.4766	0.3891
$m_{\phi\phi}$	−0.1401	−0.1687	−0.1823
$m_{r\theta}$	0.3718	−0.1971	−0.1928
$m_{r\phi}$	−0.2156	0.4265	0.3630
$m_{\theta\phi}$	0.7869	0.7773	0.8470
t_0 (s)	37.4	36.6	36.8

conclude that with our data set we would not be able to distinguish between the two models. This is in agreement with the conclusions of *Henry et al.* [2000].

[12] We compute multitaper estimates of time shifts and amplitude anomalies between data and synthetics at specific periods, as described in section 3. The results are shown in Figure 3 for periods of 207 s and 420 s for both Rayleigh and Love waves.

[13] The amplitude anomalies δ ln A_i resemble a fairly smooth sine wave pattern, positive to the west and negative to the east, that can be explained in terms of a westward propagating rupture [*Ben-Menahem*, 1961]. The time shifts $\delta\tau_i$ are near zero for all azimuths at 207 s for both Rayleigh and Love waves. At 420 s they are also near zero for westward azimuths for both wave types, but significantly different from zero in eastward azimuths. The synthetics arrive as much as 20 s earlier than the data in eastward azimuths for Rayleigh waves, and 40 s earlier for Love waves in the same azimuth. This general shape of the sinusoidal pattern of time shifts can be explained by a misrepresentation of the source [*Richter*, 1958, p. 693]. The baseline of the sinusoid is indicative of a source delay, here around 15 s, and the amplitude of the sinusoid is related to a source mislocation.

[14] These results show that the 420 s waves are consistent with a point source that occurs later and further west

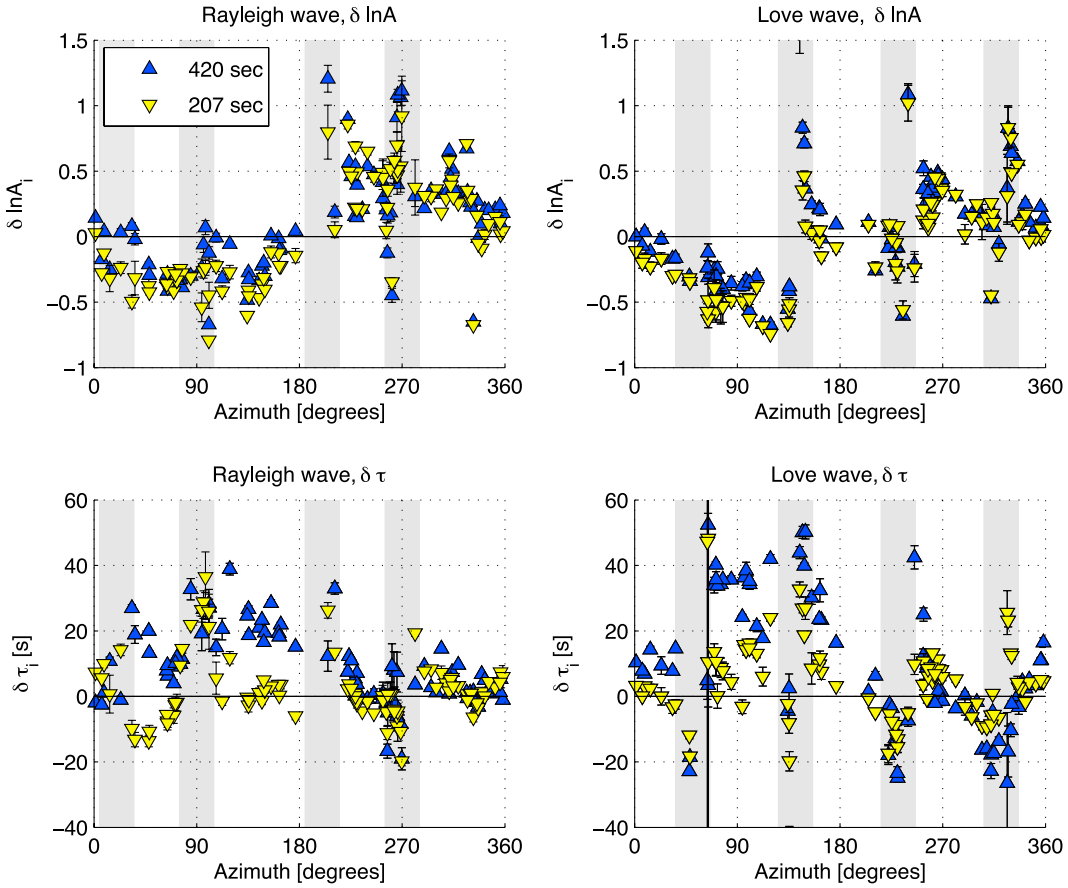

Figure 3. Multitaper measurements of amplitude anomalies and time shifts between data and synthetics for (left) Rayleigh and (right) Love waves with dominant periods of 207 (yellow triangles) and 420 s (blue triangles) computed for the Harvard best fit point source. Positive amplitudes denote larger observed ground displacements than indicated by the synthetics. Positive time shifts indicate earlier arrivals in the synthetics than in the data. Since the point source model does not account for the effects of a propagating rupture, we see a sinusoidal pattern in δ ln A: negative numbers to the west and positive numbers to the east. The pattern indicates that the main propagation of rupture was to the west. Near-nodal azimuths are shown as gray-shaded areas.

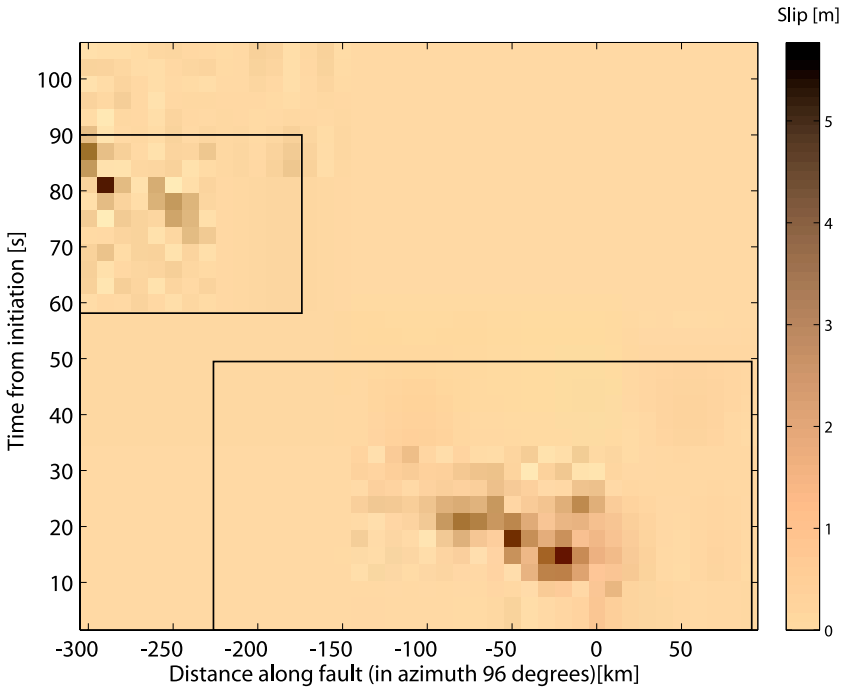

Figure 4. Source model of *Henry et al.* [2000] used in our simulations. The authors emphasize that the well-constrained parts of the solution are those in the rectangular boxes, which they refer to as subevents 1 and 2.

than the point source consistent with the 207 s waves. From this we infer that the slip (or moment) increased rapidly near the epicenter and decreased in time while propagating toward the west. The Harvard CMT was constructed to fit mantle waves with periods of 135 s and longer and does a very good job of matching the data at 207 s. If the source is localized in time and space, the point source solution is expected to fit equally well at even longer periods. The discrepancy at 420 s indicates that for this long-duration event, an even longer period cutoff is needed for point source modeling to obtain a centroid location that matches the centroid of the slip distribution.

5. Body Wave Source Model

[15] Since point source modeling indicates that a non-double-couple component, although allowable, is not needed to match the time delays and amplitude anomalies, it is of interest to see whether a purely double-couple body wave model can fit the surface waves as well. We use the source time history of *Henry et al.* [2000] to calculate 3-D synthetics for the Balleny Islands event (Figure 4).

[16] The model was obtained by inverting P and SH waves, filtered between 2 s and 120 s, for slip on two fault planes. The slip is mainly concentrated in a region within 100 km of the hypocenter, rupturing primarily to the west. In addition, there is slip around 80 s after the first event, 250 km to the west. The regions in space and time where the authors are confident in their slip models are indicated by black boxes in Figure 4.

[17] At first glance the waveforms are very well predicted by the synthetics (Figure 5). However, upon closer inspection of the very long period waves in front of the main arrival of the surface waves, it should be noted that the long-period part of the observed seismograms is not matched by the corresponding synthetics. The amplitude ratio between data and synthetics is larger for waves traveling eastward than for those traveling westward, indicating that the source model does not produce the observed amount of directivity. To quantify the differences between data and synthetics, we use the multitaper measurements of amplitude differences and time shifts (Figure 6).

[18] As observed in the waveforms, the amplitudes toward the west are under predicted, both for the Rayleigh and Love waves. However, the amplitude ratios for the Rayleigh waves do not form a simple sinusoid as a function of azimuth, as they did for the Harvard CMT. Instead, the amplitude anomalies are slightly smaller to the southwest (azimuth 225°) than to the southeast (azimuth 135°), close to zero in the northeast (azimuth 45°), and very large in the northwest (azimuth 315°). By comparing the amplitude anomalies for model HenryF (Figure 6) with the radiation patterns for the point sources (Figure 2), we infer that this is a result of using focal mechanism HenryF. This focal mechanism was obtained from body waves, and although *Henry et al.* [2000] state that the differences in misfit to the surface wave data between models HenryD and HenryF are negligible at 135 s, this indicates that, in fact, model HenryD predicts the longer-period surface waves better. We therefore repeated the simulation for the same slip model but using surface wave focal mechanism HenryD. The waveforms for this model are shown in Figure 7 and the amplitude anomalies and time shifts are shown in Figure 8.

[19] The pattern of amplitude anomalies for the Rayleigh wave is now similar to that for the Harvard CMT, although offset by a constant, with positive anomalies in the easterly

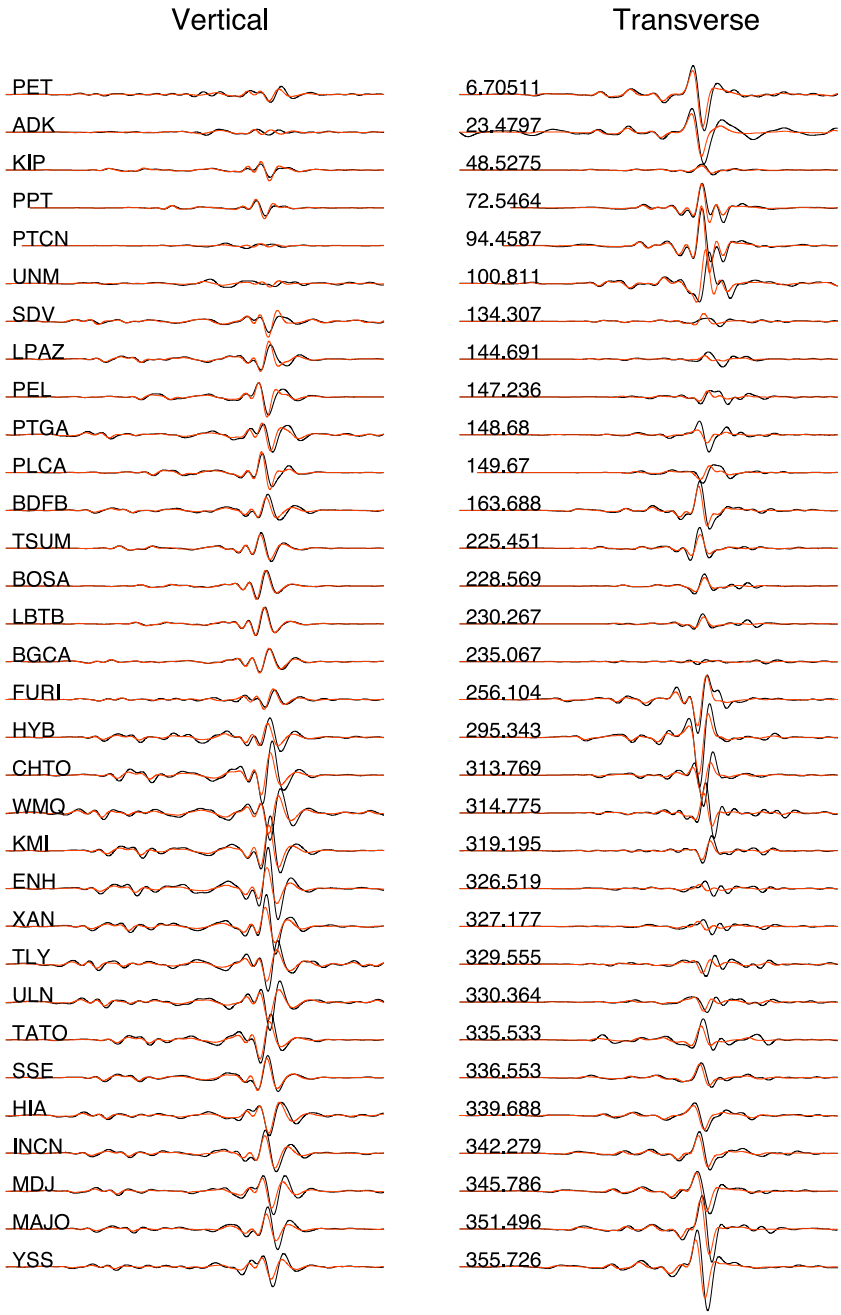

Figure 5. Waveforms computed for model HenryF. Data are shown in black, and the 3-D synthetics are shown in red. All traces have been band-pass-filtered between 100 and 500 s. The vertical component is shown on the left, and the transverse component is shown on the right. The 3000 s long records are aligned on the arrival of the Rayleigh or Love waves on the vertical and transverse components, respectively. Station names are shown with the vertical component, and azimuths are shown with the transverse component. The synthetics to the west are generally small compared to the observed ground displacements, and overall the synthetics are slightly early relative to the observed seismograms.

direction. A similar pattern can be discerned for the Love wave, although the measurements near the nodal directions (in the shaded regions) show significant variations. Notice that almost all the amplitude anomalies are positive, indicating that the model has a moment that is smaller than needed to explain the observed amplitudes. The time shifts for both Rayleigh and Love waves indicate an earlier arrival than observed in all directions, and more so in the west than in the east. This indicates that there is significant slip at later times than predicted by the body wave model.

6. Modification of the Body Wave Model

[20] Since the overall amplitudes of the synthetics for the finite source model with focal mechanism HenryD match the body waves and short-period surface waves (Figure 7)

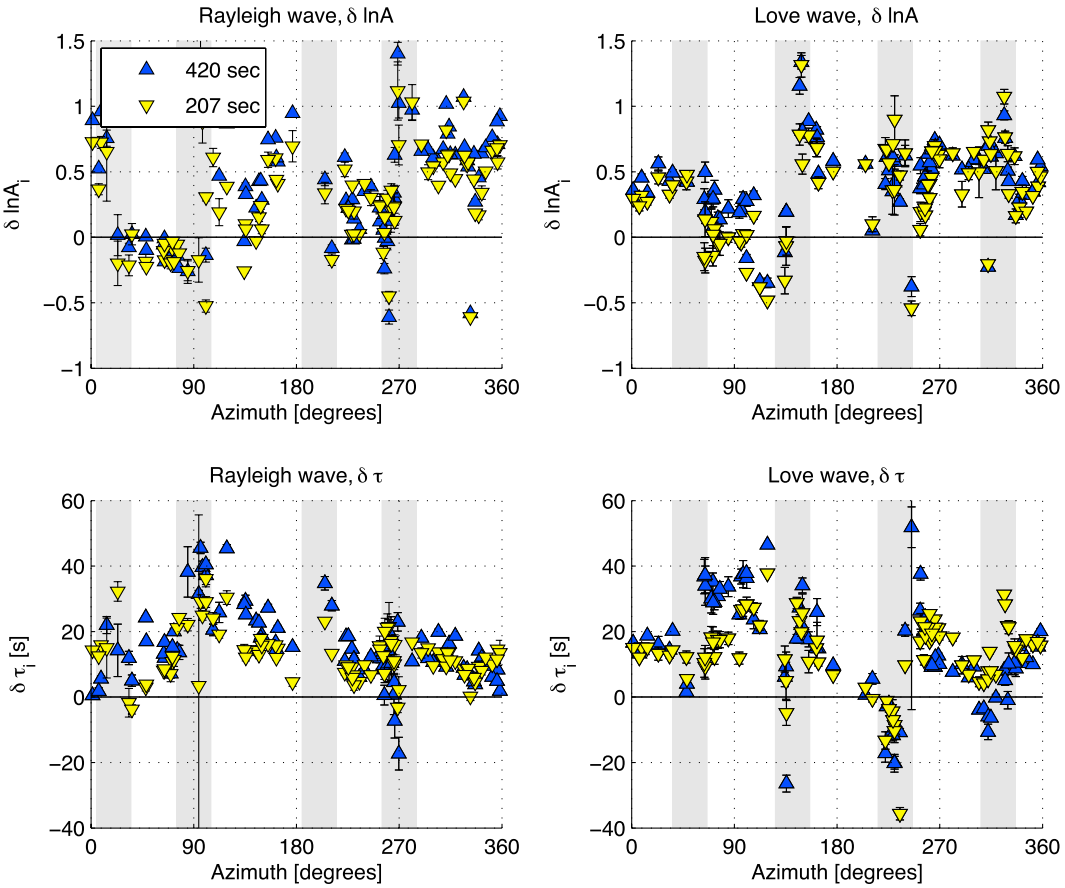

Figure 6. Multitaper measurements of amplitude anomalies and time shifts between data and synthetics for (left) Rayleigh and (right) Love waves with dominant periods of 207 (yellow triangles) and 420 s (blue triangles) for the *Henry et al.* [2000] source model (Figure 4) with focal mechanism HenryF. Note that almost all of the amplitude measurements are positive, indicating that the amplitudes of the long-period seismic waves are underestimated by this model. Note also that the directivity is underestimated as well (the amplitude ratios are azimuthally dependent). Nodes in the Rayleigh and Love wave radiation patterns are indicated by the gray-shaded areas.

reasonably well, but not the long-period mantle waves (Figure 8), we can exclude the possibility that the source time function simply underestimates the total moment and thus that a better fit would be achieved by scaling it by a constant. Furthermore, the observed time shifts indicate that the missing slip occurs at a later time than the main slip prescribed in the body wave model.

[21] The lack of long-period energy in the synthetics computed on the basis of the body wave model is not surprising when we consider that the data used for the body wave inversion were band passed between 2 s and 120 s, and thus the very long period energy in the body waves was filtered out. Furthermore, body wave inversions are known to be insensitive to the long-period components of slip and therefore to the moment of an earthquake [*Ekström*, 1989]. We would like to find a model that can explain the data over the entire frequency range, and, building on the earlier results, we thus need to add a component that augments the amplitude of the signal at long periods but does not affect the shorter periods. One way of doing this is to assume that the two subevents described by *Henry et al.* [2000] are on a single fault plane and modify their model by adding slip between the two distinct fault patches. We accomplish this by adding slip to the fault with a moment rate function of the form: $\dot{M}(t) = \Delta M_0\ (\pi/2T)\sin(\pi t/T)$, $t \in [0,T]$, where ΔM_0 is the total moment of the added slip and T is the duration of the rupture. The slip is assumed to propagate along the entire fault with a fixed rupture speed of $300/T$ km/s (Figure 9). Adding long-period slip to body wave source inversions to match the moment obtained from surface wave amplitudes was common practice in the late 1980s [e.g., *Kikuchi and Fukao*, 1987; *Beck and Ruff*, 1987], when interpreting body waves recorded by the WWSSN network, which had limited bandwidth. Because of the insensitivity of body waves to long-period components of slip, however, this is still a useful practice in the age of modern digital seismology.

[22] Notice that two free parameters are involved: the added moment, ΔM_0, and the duration of rupture, T. We experimented with both, using trial and error, to obtain

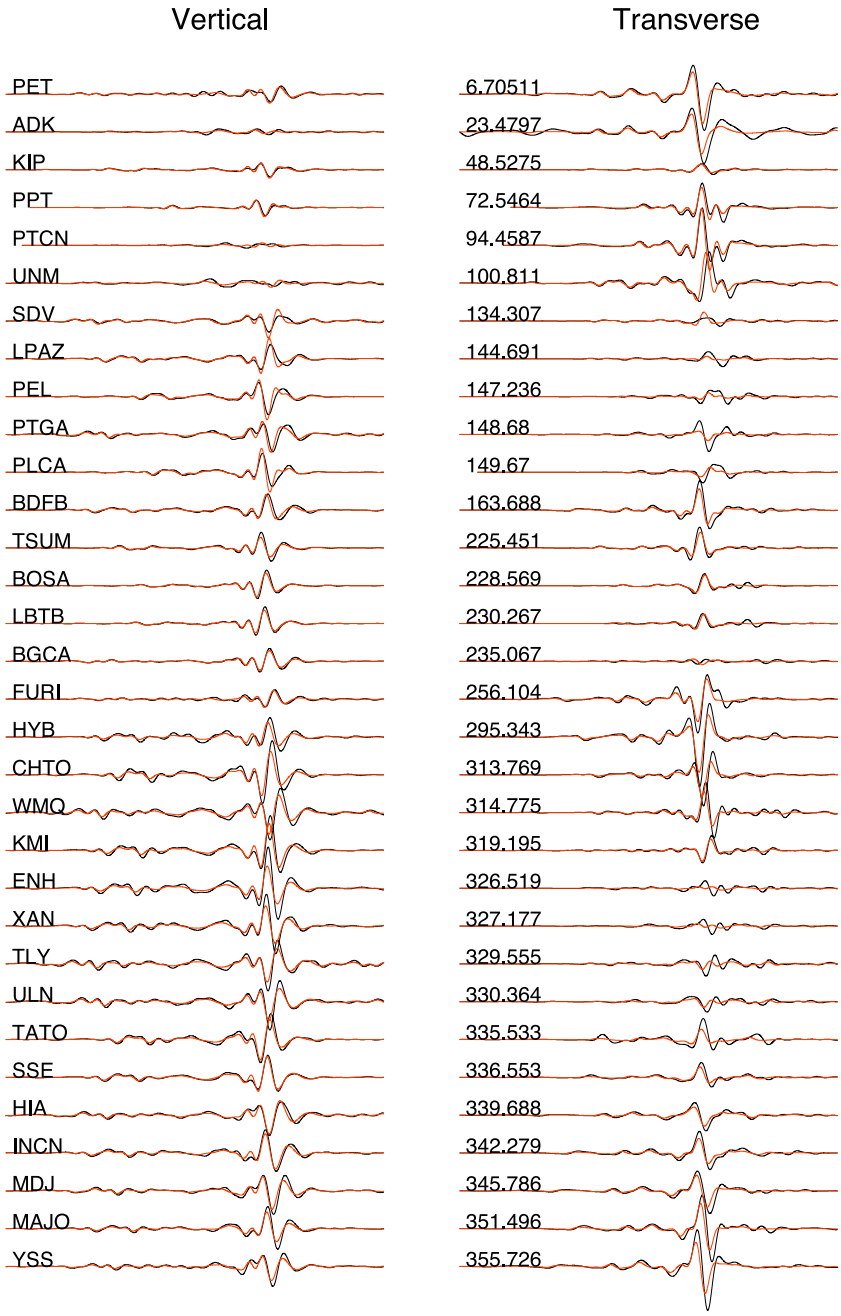

Figure 7. Waveforms computed for model HenryD. Data are shown in black, and the 3-D synthetics are shown in red. All traces have been band-pass-filtered between 100 and 500 s. The vertical component is shown on the left, and the transverse component is shown on the right. The records are 3000 s in duration and aligned on the arrival of the Rayleigh and Love waves on the vertical and transverse components, respectively. Station names are shown with the vertical component, and azimuths are shown with the transverse component.

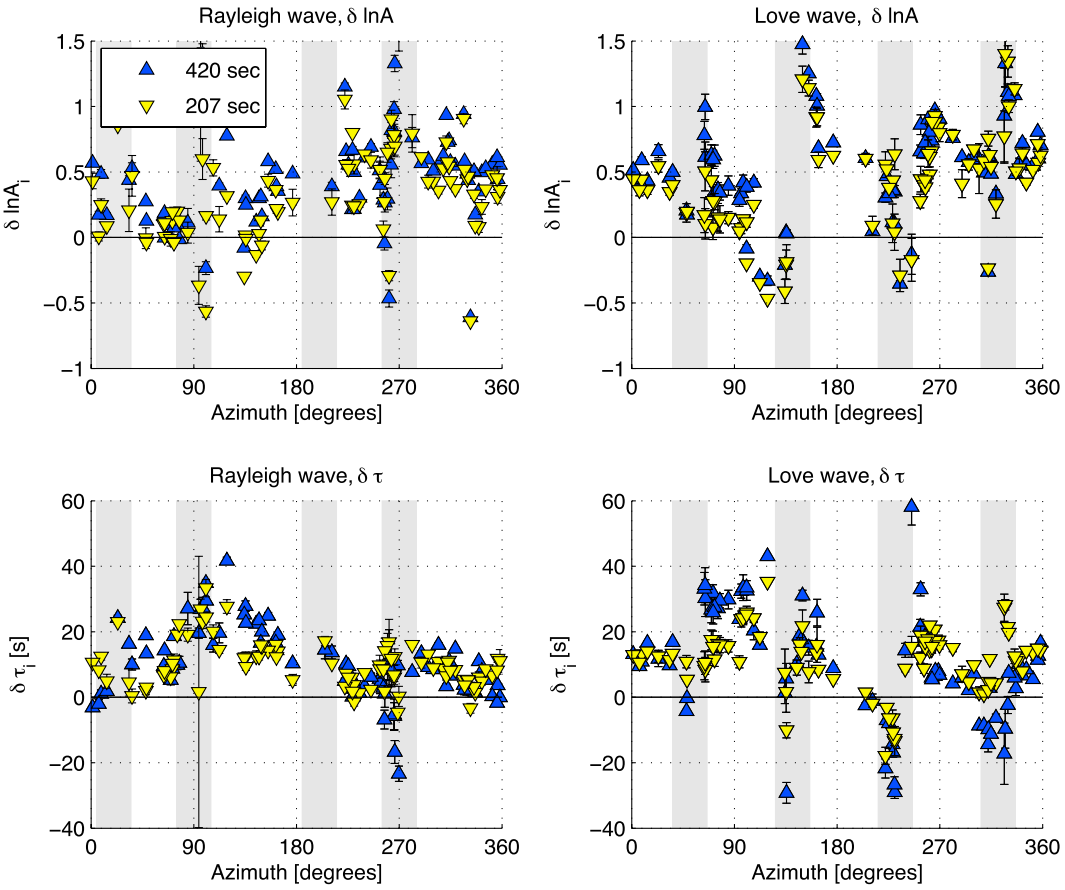

Figure 8. Multitaper measurements of amplitude anomalies and time shifts between data and synthetics computed for the *Henry et al.* [2000] source model (Figure 4) with focal mechanism HenryD. The main differences between using focal mechanisms HenryD and HenryF are seen in the amplitude ratios of the Rayleigh wave. The amplitude ratio is now more similar to a simple sinusoid, indicating that the remaining discrepancy is due to how the rupture propagates along the fault plane, not the geometry thereof.

good fits to the long-period radiation pattern. We found that $\Delta M_0 = 8 \times 10^{20}$ Nm and $T = 100$ s give the best fits. The duration of rupture in the original model is $T = 90$ s, but that gives a slightly worse fit to the time shifts. The waveforms for this new model are shown in Figure 10 and the multitaper measurements are shown in Figure 11.

[23] On average the time shifts and amplitudes of both Rayleigh and Love waves are close to zero. There are significant variations in the nodal regions, indicating that perhaps we could obtain better fits by a slight rotation of the strike of the event. Comparing Figures 3 and 8, we see that the model with an added component of smooth slip has smaller amplitude anomalies and time shifts than the other finite fault models at both 207 s and 420 s.

[24] To demonstrate that the modified source model has similar fits to the observed body waves as the original model we compute P and SH waveforms for both source models. We use a Haskell propagator matrix to compute the response at the source and receiver sides [*Bouchon*, 1976; *Haskell*, 1960, 1962]. The waveforms are band-pass-filtered between 2 and 120 s using a four pole, two pass Butterworth filter. The results are shown in Figure 12. The waves are in fact nearly indistinguishable at all azimuths. By using a low pass at 300 s small differences were visible at nearby stations in the rupture direction (WRAB and NWAO), but the differences were considerably smaller than between the synthetics and the observed data. We therefore conclude that one cannot distinguish between the original model and the modified model on the basis of body waves alone.

7. Discussion

[25] We computed long-period synthetics for a pure double-couple body wave source model of the Balleny Islands event with two distinct rupture patches [*Henry et al.*, 2000], but find that the model predicts much smaller amplitudes at long periods than observed. We present a modification of the *Henry et al.* [2000] source model that incorporates long-period slip along a fault plane that connects and incorporates the two patches. The need for this added slip can be appreciated by looking at the moment rate functions for the different models (Figure 13). The Harvard

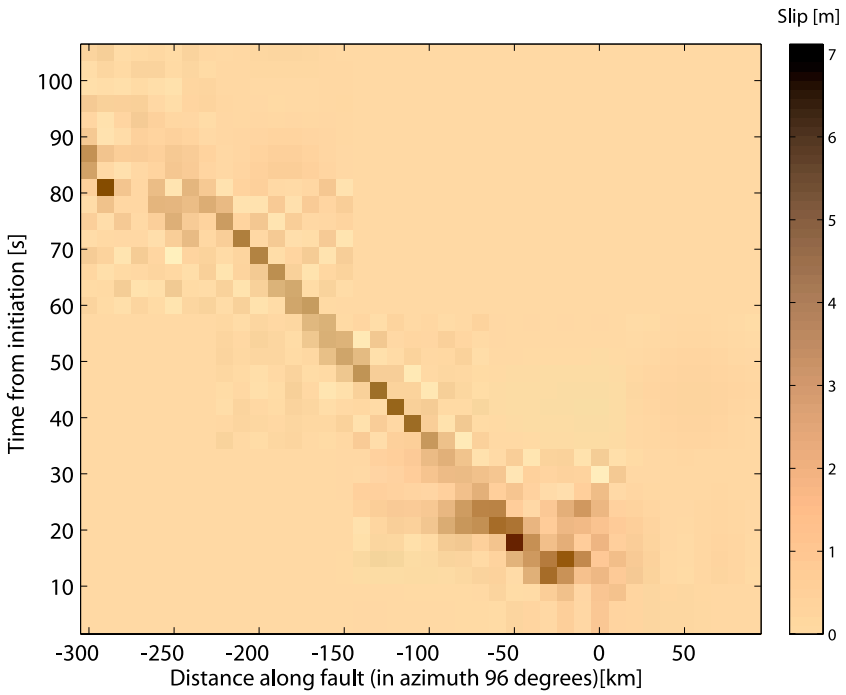

Figure 9. Slip model modified from *Henry et al.* [2000] to fit the long-period radiation pattern better. Point sources are added in a smooth manner along the line representing a constant rupture speed of 3.0 km/s as described in the text.

CMT solution is the point source that best fits the long-period data, in this case mantle waves low-pass filtered at 135 s. The source has a boxcar source time function (here represented by a Gaussian to minimize the generation of numerical noise) with a half duration that is scaled on the basis of the moment (Figure 13). In the ideal case, the center of the box car coincides with the first moment of the moment rate function of the earthquake. Upon comparing the moment rate function of the Harvard CMT solution and the one by *Henry et al.* [2000], we can immediately see that the centroid of the second model is significantly earlier than suggested by the long-period data. Comparing the source spectra, we can see that the difference between the original finite rupture model and the modified model only appears at 80 s and longer, indicating that both models will fit the body waves equally well. We can also see that at 207 s we are not yet at the flat part of the spectra for the kinematic rupture models.

[26] We can give a more quantitative measure of the quality of fit of the models by using the definitions of $\overline{\delta \ln A}$ and $\overline{\delta \tau}$. These values, averaging over all azimuths and periods between 100 s and 500 s are given in Figure 14. The average amplitude anomalies are close to zero for both the Harvard CMT solution and the modified finite fault model. However, the HenryD and HenryF finite fault models have large average time shifts and amplitude anomalies. The variations around the averages are largest for the Harvard CMT solution and smallest for the modified finite model.

[27] Using synthetics computed for a 3-D structure allows us to interpret the measurements of phase shifts and amplitude anomalies in terms of source effects, rather than structural effects, in the period range 100–500 s. However, the main conclusions of this paper are not critically dependent on the 3-D Earth model as the discrepancies between the two-subevent model and the continuous model are largest at long periods, where waveforms are well modeled by spherical Earth models.

[28] Because the modified source model has continuous slip along one single fault plane, it is by some measure the simplest model that has been shown to fit both body waves and long-period surface waves. The model by *Kuge et al.* [1999] is composed of five nearly pure strike-slip events, the first three corresponding to the first subevent in this study, and the last two corresponding to the second subevent. In order to fit the non-double-couple component they add three normal faulting subevents, with long rupture duration, at the ends of the strike-slip events. The long duration is needed to reduce the body wave radiation from the normal subevents, as they are much more efficient at radiating far-field P waves than strike-slip subevents. In this model there is a 60 km gap between the two clusters of subevents. This setting is explained in terms of a series of en echelon strike-slip faults connected by normal faulting events.

[29] *Nettles et al.* [1999] model the Balleny Islands earthquake in terms of five nearly pure strikes-slip events, but point out that the last two have a $10 \pm 5^\circ$ counterclockwise rotation in strike, going from 281° to 271°, relative to the first three. They suggest this could indicate a curved fault or two faults slightly offset from each other. They

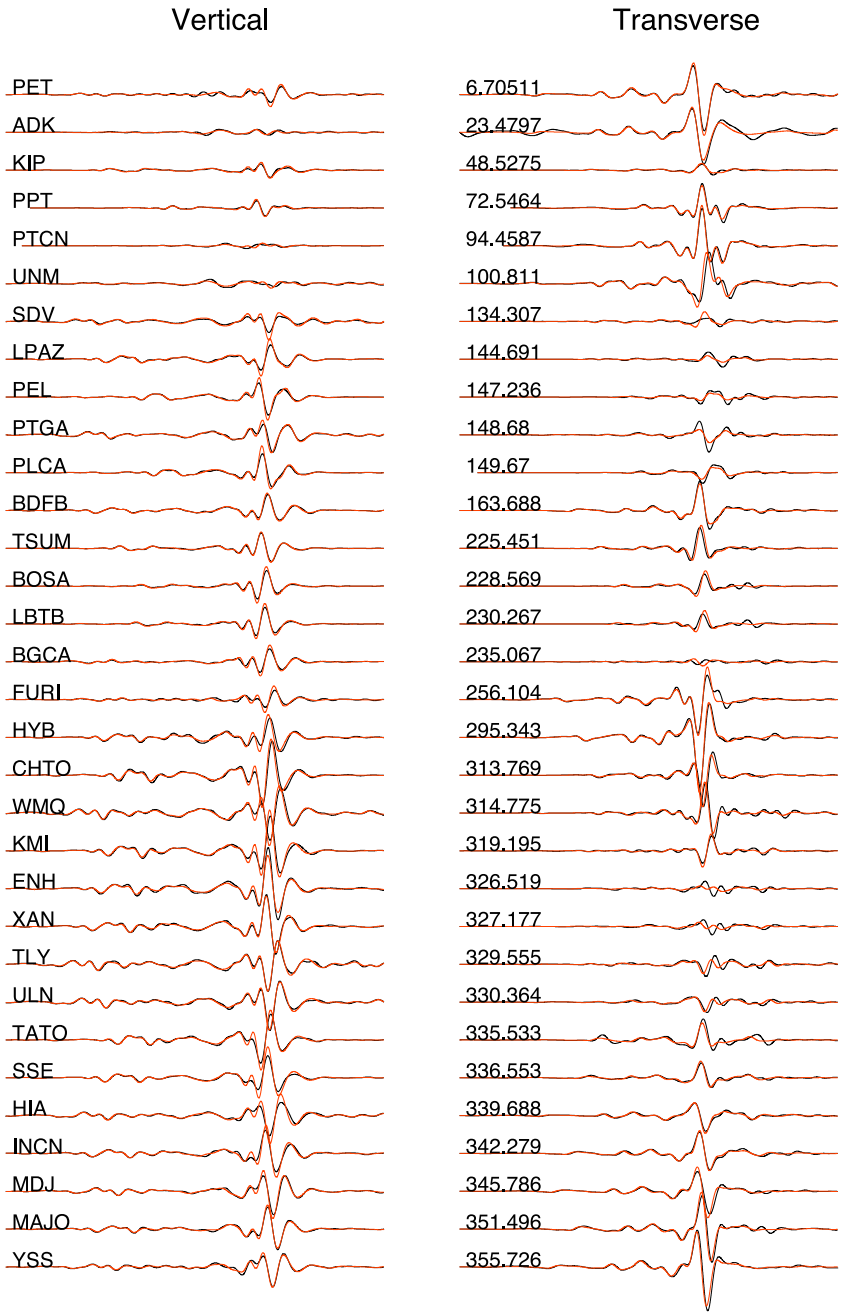

Figure 10. Same as Figure 7 except with synthetics computed for the modified source model. The amplitude and phase of the surface waves match the data better than for the previous models. Furthermore, the earlier phases, which were not used to constrain the model, are also better matched.

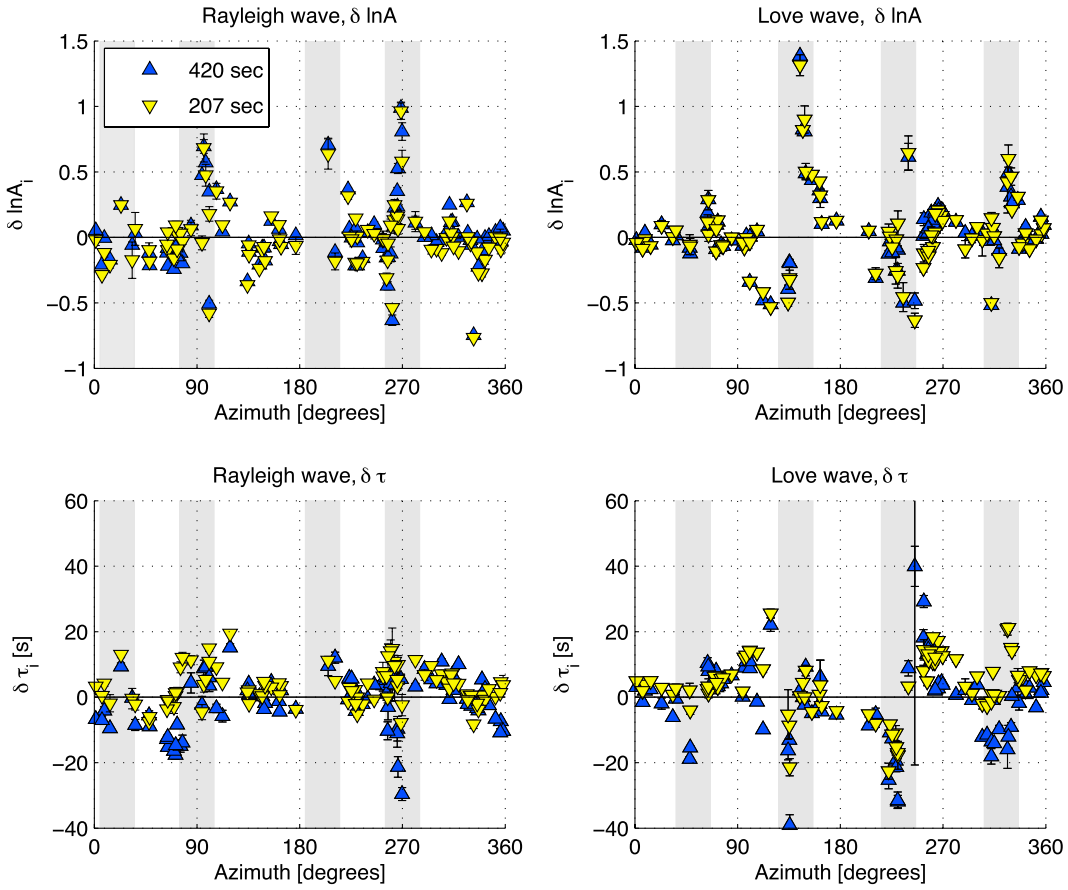

Figure 11. Multitaper measurements of amplitude anomalies and time shifts for the modified *Henry et al.* [2000] source model (Figure 9). On average, all of the measurements are close to zero for both Rayleigh and Love waves at both periods of 207 (yellow triangles) and 420 s (blue triangles), reflecting close agreement between observed and predicted waveforms except near nodes in the radiation patterns, indicated by the gray-shaded areas.

make no attempt to explain the non-double-couple component, and by comparison to the studies of *Kuge et al.* [1999] and *Henry et al.* [2000] it is unlikely that this purely strike-slip solution would explain the long-period data. By using finite fault modeling of body waves, *Antolik et al.* [2000] suggest that the non-double-couple component of the Harvard CMT solution may be explained by compound rupture on two faults: one nearly pure strike slip fault, consistent with the first motions, and the other an oblique normal fault rotated $\sim$25° relative to the first. Both *Antolik et al.* [2000] and *Henry et al.* [2000] point out that the first motions of the P wave require that the rupture started as nearly pure strike slip.

[30] Oceanic earthquakes occur mostly on vertical strike slip faults which are connected by normal faults. Therefore it may seem somewhat puzzling that this 300 km long fault could have a dip and rake as large as suggested by the surface wave modeling. However, large strike-slip faults in continental settings, such as the Kunlun fault in China and the Denali fault in Alaska, are thought to have, at least locally, nonvertical dip and rake angles [*Ozacar and Beck*, 2004; *Antolik et al.*, 2004], and therefore we do not find the nonvertical dip and nonhorizontal rake angle inconceivable for this large event.

[31] As described above, other studies have suggested a combination of normal faulting and strike-slip faulting to explain the source mechanism of the Harvard CMT solution. As the surface wave amplitudes and time shifts can be equally well matched by the focal mechanism in this study (in agreement with *Henry et al.* [2000]), we do no exclude these fault models but conclude that the faulting geometry may be simpler than suggested by these authors.

[32] The continuity of slip is important, as a large unbroken patch between the two subevents implies dynamic triggering over a large distance. Our result, that there is slip between the two subevents, indicates that the standard mechanism, in which rupture propagation is driven by stress concentration at a crack tip, suffices to explain this event.

8. Conclusions

[33] We have compared observed surface waves for the 1998 Balleny Islands event to simulations for four different source models: one surface wave point source model (the Harvard CMT solution of *Dziewonski et al.* [2003]), one

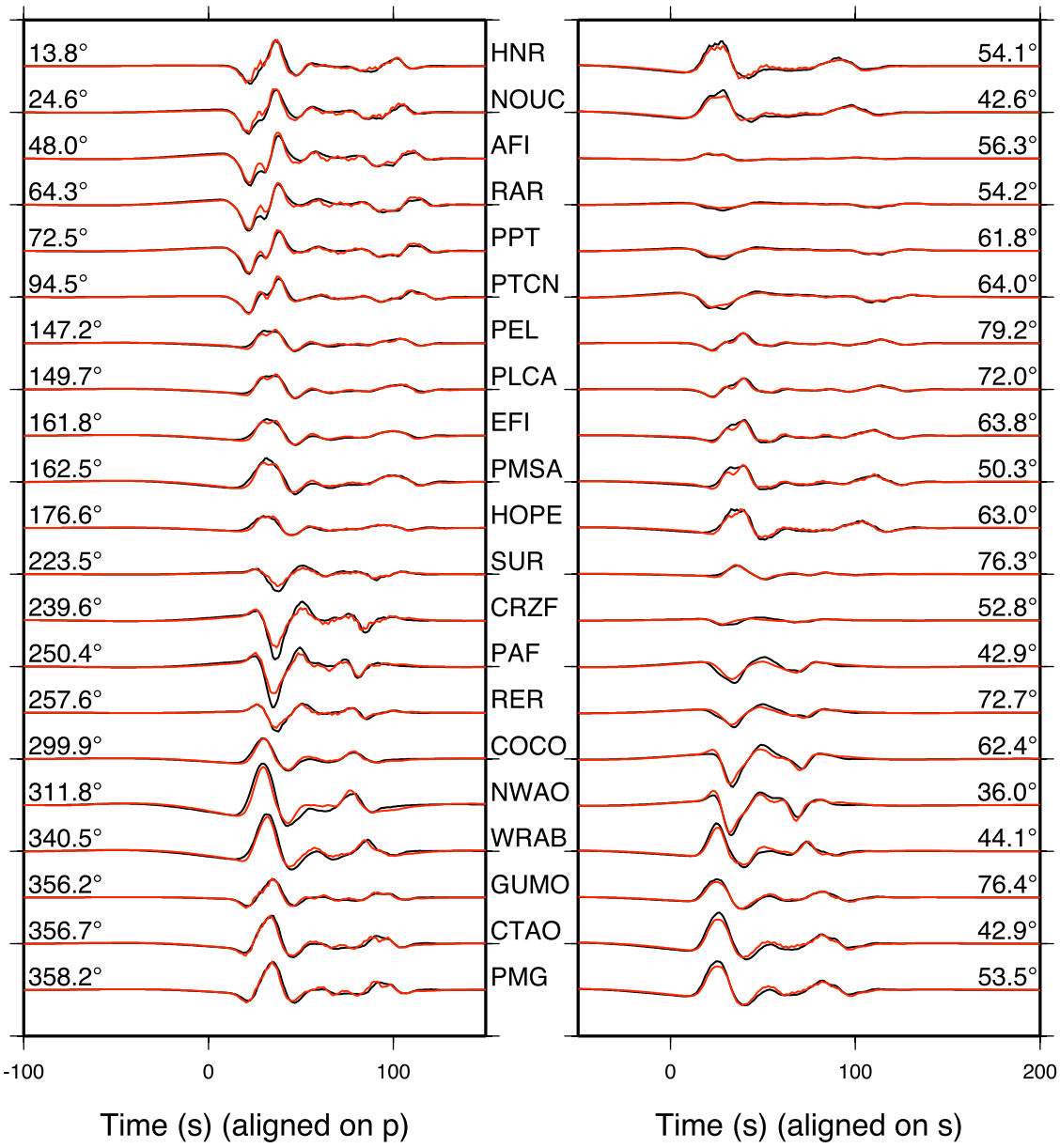

Figure 12. (left) Vertical and (right) transverse displacement seismograms for the two-subevent source model of *Henry et al.* [2000] (black) and a version of the same model where slip has been added, connecting the two subevents (red). The seismograms are band-pass-filtered at periods between 2 and 120 s. The azimuth from the epicenter to receiver is shown on the left, the epicentral distance in degrees is on the right, and the station names are in the middle.

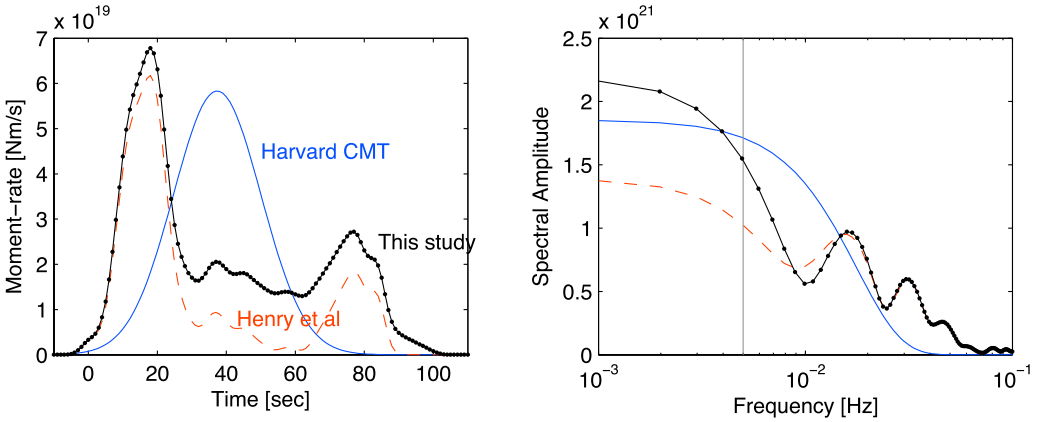

Figure 13. Moment rate functions for the models discussed in this paper in the (left) time and (right) frequency domains. The vertical gray line in the right plot at 200 s indicates that at this period we are still not at the flat part of the spectrum.

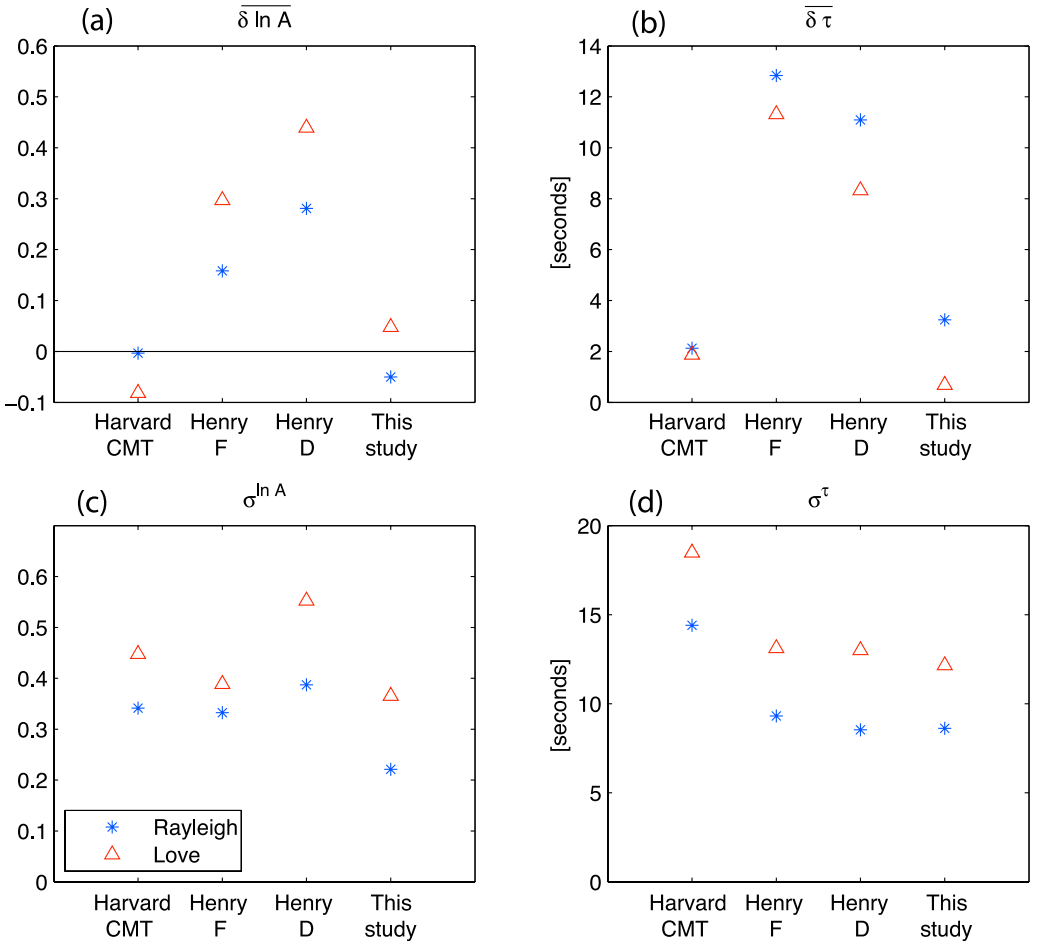

Figure 14. Multitaper measurements averaged over all azimuths and over a period band between 100 and 500 s. The models are the Harvard CMT solution (Harvard CMT), the finite source model with focal mechanism HenryF (Henry F), the finite source model with focal mechanism HenryD (Henry D), and the modified finite model with focal mechanism HenryD (this study). (a) Average amplitude anomaly $\overline{\delta \ln A}$. (b) Average time shift $\overline{\delta\tau}$ calculated on the basis of (6). (c) Variation around the average amplitude anomaly $\sigma^{\ln A}$. (d) Variation around the average time shift σ^{τ} calculated on the basis of (7).

finite fault model with two different focal mechanisms (models HenryD and HenryF of *Henry et al.* [2000]) and one finite fault model that combines model HenryD and a smooth component of slip extending over the whole fault, propagating unilaterally. We have shown that by adding this component of slip we can significantly improve the fits to the amplitude and phase of global surface waves. The modified body wave model provides reasonable fits to long-period surface waves as well as body waves, without invoking slip on multiple fault planes or on unconnected fault patches. The continuity of slip indicates that this event can be explained by standard fracture mechanics models where the rupture is driven by the stress concentration at the crack tip. We have only proven the existence of such a model, not its uniqueness. We present this as the simplest model that gives a reasonable match to a wide range of data sets, although a more segmented rupture cannot be ruled out.

[34] This study emphasizes the importance of including long-period waves in finite fault modeling. The most basic approach is to constrain the models to have the correct moment, centroid time, and location. Here we further match the azimuthal amplitude pattern due to the directivity of the rupture. Care has to be taken to use waves that have periods several times longer than the duration of the source to properly estimate the point source parameters. By combining body wave modeling with surface wave modeling we retain both the robustness provided by the surface waves and the detail contained in the body waves.

[35] **Acknowledgments.** We acknowledge support by the National Science Foundation under grant EAR-0711177. This is Seismolab contribution 10013. The numerical simulations for this research were performed on Caltech's Division of Geological and Planetary Sciences Dell cluster. We thank Göran Ekström for helpful suggestions. The comments of Keiko Kuge and an anonymous reviewer improved the manuscript.

References

Antolik, M., A. Kaverina, and D. S. Dreger (2000), Compound rupture of the great 1998 Antarctic plate earthquake, *J. Geophys. Res.*, *105*, 23,825–23,838.

Antolik, M., R. E. Abercrombie, and G. Ekström (2004), The 14 November 2001 Kokoxili (Kunlunshan), Tibet, earthquake: Rupture transfer through a large extensional step-over, *Bull. Seismol. Soc. Am.*, *94*(4), 1173–1194.

Bassin, C., G. Laske, and G. Masters (2000), The current limits of resolution for surface wave tomography in North America, *EOS Trans. AGU*, *81*(48), Fall Meet. Suppl., Abstract S12A-03.

Beck, S. L., and L. J. Ruff (1987), Rupture process of the great 1963 Kuril Islands earthquake sequence: Asperity interaction and multiple event rupture, *J. Geophys. Res.*, *92*, 14,123–14,138.

Ben-Menahem, A. (1961), Radiation of seismic surface-waves from finite moving sources, *Bull. Seismol. Soc. Am.*, *51*(3), 401–435.

Ben-Menahem, A., and D. Harkrider (1964), Radiation patterns of seismic surface waves from buried dipolar point sources in a flat stratified Earth, *J. Geophys. Res.*, *69*, 2605–2620.

Bouchon, M. (1976), Teleseismic body wave radiation from a seismic source in a layered medium, *Geophys. J. R. Astron. Soc.*, *47*, 515–530.

Dziewonski, A. M., G. Ekström, and N. N. Maternovskaya (2003), Centroid-moment tensor solutions for January to March 1998, *Phys. Earth Planet. Inter.*, *136*, 133–144.

Ekström, G. (1989), A very broad band inversion method for the recovery of earthquake source parameters, *Tectonophysics*, *166*, 73–100.

Hartzell, S. H., and T. H. Heaton (1983), Inversion of strong ground motion and teleseismic waveform data for the fault rupture history of the 1979 Imperial Valley, California, earthquake, *Bull. Seismol. Soc. Am.*, *73*(6A), 1553–1583.

Haskell, N. A. (1960), Crustal reflection of plane *SH* waves, *J. Geophys. Res.*, *65*, 4147–4150.

Haskell, N. A. (1962), Crustal reflection of plane *P* and *SV* waves, *J. Geophys. Res.*, *67*, 4751–4767.

Henry, C., S. Das, and J.H. Woodhouse (2000), The great March 25, 1998, Antarctic plate earthquake: Moment tensor and rupture history, *J. Geophys. Res.*, *105*, 16,097–16,118.

Kanamori, H., and J. Given (1981), Use of long-period surface waves for rapid determination of earthquake-source parameters, *Phys. Earth Planet. Inter.*, *27*, 8–31.

Kikuchi, M., and Y. Fukao (1987), Inversion of long-period *P*-waves from great earthquakes along subduction zones, *Tectonophysics*, *144*, 231–247.

Kikuchi, M., and H. Kanamori (1991), Inversion of complex body waves—III, *Bull. Seismol. Soc. Am.*, *81*(6), 2335–2350.

Komatitsch, D., and J. Tromp (2002a), Spectral-element simulations of global seismic wave propagation—I. Validation, *Geophys. J. Int.*, *149*(2), 390–412.

Komatitsch, D., and J. Tromp (2002b), Spectral-element simulations of global seismic wave propagation—II. Three-dimensional models, oceans, rotation and self-gravitation, *Geophys. J. Int.*, *150*(1), 303–318.

Kuge, K., M. Kikuchi, and Y. Yamanaka (1999), Non-double-couple moment tensor of the March 25, 1998, Antarctic earthquake: Composite rupture of strike-slip and normal faults, *Geophys. Res. Lett.*, *26*(22), 3401–3404.

Laske, G., and G. Masters (1996), Constraints on global phase velocity maps from long-period polarization data, *J. Geophys. Res.*, *101*, 16,059–16,075.

Nettles, M., T. C. Wallace, and S. L. Beck (1999), The March 25, 1998 Antarctic plate earthquake, *Geophys. Res. Lett.*, *26*(14), 2097–2100.

Ozacar, A. A., and S. L. Beck (2004), The 2002 Denali fault and 2001 Kunlun fault earthquakes: Complex rupture processes of two large strike-slip events, *Bull. Seismol. Soc. Am.*, *94*(6B), S278–S292.

Richter, C. F. (1958), *Elementary Seismology*, W. H. Freeman, San Francisco, Calif.

Ritsema, J., H. J. van Heijst, and J. H. Woodhouse (1999), Complex shear wave velocity structure imaged beneath Africa and Iceland, *Science*, *286*(5446), 1925–1928.

Slepian, D. (1978), Prolate spheroidal wave funtions, Fourier analysis, and uncertainty. V: The discrete case, *Bell Syst. Tech. J.*, *57*, 1371–1430.

Thomson, D. (1982), Spectrum estimation and harmonic analysis, *Proc. IEEE*, *70*, 1055–1096.

Tsuboi, S., M. Kikuchi, Y. Yamanaka, and M. Kanao (2000), The March 25, 1998 Antarctic earthquake: Great earthquake caused by postglacial rebound, *Earth Planets Space*, *52*(2), 133–136.

Zhou, Y. (2004), Surface wave propagation in laterally heterogeneous media: With application to global upper-mantle tomography, Ph.D. thesis, Princeton Univ., Princeton, N. J.

V. Hjörleifsdóttir, Lamont-Doherty Earth Observatory, P.O. Box 1000,61 Route 9W, Palisades, NY 10964-8000, USA. (vala@ldeo.columbia.edu)

H. Kanamori, Seismological Laboratory, Division of Geological and Planetary Sciences, California Institute of Technology, Pasadena, CA 91125, USA.

J. Tromp, Department of Geosciences, Princeton University, Princeton, NJ 08544, USA.